ACTA MONTANA IRSM AS CR (1998)
Series A No.12(107), 115–124

COMPUTATION OF RAY AMPLITUDES IN RADIALLY INHOMOGENEOUS MEDIA WITH SLOPING EARTH SURFACE

JAROMÍR JANSKÝ

Department of Geophysics, Faculty of Mathematics and Physics, Charles University
Ke Karlovu 3, 121 16 Prague 2, Czech Republic

ABSTRACT. A program for computation of three–component ray synthetic seismograms in radially inhomogeneous media was modified to account for sloping Earth surface. The amplitude record can be significantly different in this case as compared to the case of spherical surface. The dominant part of this difference is due to the free surface conversion coefficient. The 3–D influence of the free–surface slope in relation to the azimuth and angle of the incidence of the P wave to the recorded vertical and horizontal components of displacement is demonstrated in this paper.

KEYWORDS: Conversion coefficient, free–surface slope and azimuth, P wave, displacement amplitude, ray method.

1. INTRODUCTION

The program package ZESMO (Zedník at al., 1993) was designed for fast interactive computation of three–component body wave synthetic–ray seismograms in radially inhomogeneous media and for displaying them along with observed seismograms. This program package was developed as a contribution to the objectives of the ISOP project (Engdahl, 1989).

Recently a part of package mentioned was modified to account for sloping Earth surface. The amplitude record can be significantly different in this case as compared to the case of spherical surface. The dominant part of this difference is due to the free–surface conversion coefficient. The 3–D influence of the free surface – mountain slope in relation to the azimuth and angle of the incidence of the P wave to the recorded vertical and horizontal components of displacement is demonstrated in this paper.

In demonstration we suppose that the mountain size and its radii of curvature are sufficiently large, compared to the prevailing wavelength of the incident wave, in order to use the ray method. In the computation we have limited ourselves to the simple form of mountain only. Influence of the more complicated mountain structure, influence of possible multiple wave reflections inside the mountain, etc. were not taken into consideration.

The rather strong influence of the free–surface conversion coefficient is due to the fact that in the case of mountain slope we compute the components of displacement in the rotated coordinate system, connected with the mountain slope – taken as

the new "surface plane" – whereas the coordinate system of recording is connected with the horizontal surface.

We work with displacement in this contribution, but similar results are valid for velocity or acceleration components as well. We assume that the mountain density, wave velocity and quality parameter are constant and identical to these parameters for the upper crustal layer in the Earth model used.

The mentioned mountain form, of course, influences the travel times, and can cause shadow zones. These phenomena were not studied in this contribution, too.

Earth flattening approximation (Müller, 1977) has been applied in program ZESMO and the Cartesian coordinate system is used in the following computations.

2. Method of Computation

Let us introduce a rectangular coordinate system X, Y, Z with its origin at the recording point (at the seismic station), Z axis being oriented positive upwards. The ray of incident wave is situated in the vertical plane XZ and is represented by the tangential unit vector $\boldsymbol{t}$ at the point of incidence (at the recording point). The x component of this tangential vector is assumed to be positive. Vector $\boldsymbol{t}$ and axis Z make the acute "incidence angle" i.

Let us have plane S, which is tangent to the mountain surface at the recording point (at the point of the ray incidence). This plane is defined by its slope d, i.e. by the acute angle between the outer normal $\boldsymbol{n}$ to S (at the recording point) and the axis Z, and by the trend a. Trend a is an angle in the XY plane, made by the X axis and the projection of the normal $\boldsymbol{n}$ into the XY plane. Trend a, measured positively counterclockwise from X, represents the relation between the mountain and incident wave azimuths. (See Fig.1). Formally we consider $0 \leq d \leq \pi/4$, $0 \leq a \leq \pi$ rad.

Let us suppose, that the incident wave has an unit displacement amplitude. In the case of horizontal surface ($d = 0$, a is not defined) the free–surface conversion coefficient gives the recorded vertical $\boldsymbol{A}_V$ and horizontal $\boldsymbol{A}_H$ displacement components of the incident P wave as a function of the wave incidence angle i only. Here $\boldsymbol{n}$ and $\boldsymbol{A}_V$ are parallel to Z and $\boldsymbol{A}_H$ is parallel to X.

For $d > 0$, the conversion coefficient is applied under conditions that the plane of the incident wave is given by $\boldsymbol{t}$ and $\boldsymbol{n}$, and that the new incidence angle i', in relation to $\boldsymbol{n}$, is estimated as $\cos i' = (\boldsymbol{t} \cdot \boldsymbol{n})$. Displacement component given now by the free–surface conversion coefficient as the "vertical" one $\boldsymbol{A}'_V$ will be parallel to $\boldsymbol{n}$, the "horizontal" displacement component $\boldsymbol{A}'_H$ will be parallel to $\boldsymbol{h} = [\boldsymbol{n} \times [\boldsymbol{t} \times \boldsymbol{n}]]$. Both vectors i.e. $\boldsymbol{A}'_V$ and $\boldsymbol{A}'_H$ have components to the Z axis and to the XY plane. Let us mark the sum of contributions from $\boldsymbol{A}'_V$ and $\boldsymbol{A}'_H$ into Z as $\boldsymbol{A}^*_V$, and the sum of contributions from $\boldsymbol{A}'_V$ and $\boldsymbol{A}'_H$ into the plane XY as $\boldsymbol{A}^*_H$. $\boldsymbol{A}^*_H$ has, contrary to the $\boldsymbol{A}_H$, generally non–zero component to Y. $\boldsymbol{A}^*_V$ and $\boldsymbol{A}^*_H$ are vertical and horizontal components of displacement recorded by the seismic station, due to the standard Z, NS and EW orientation of the 3 component seismograph. The difference between mod $\boldsymbol{A}^*_V$ and mod $\boldsymbol{A}_V$ and the difference between mod $\boldsymbol{A}^*_H$

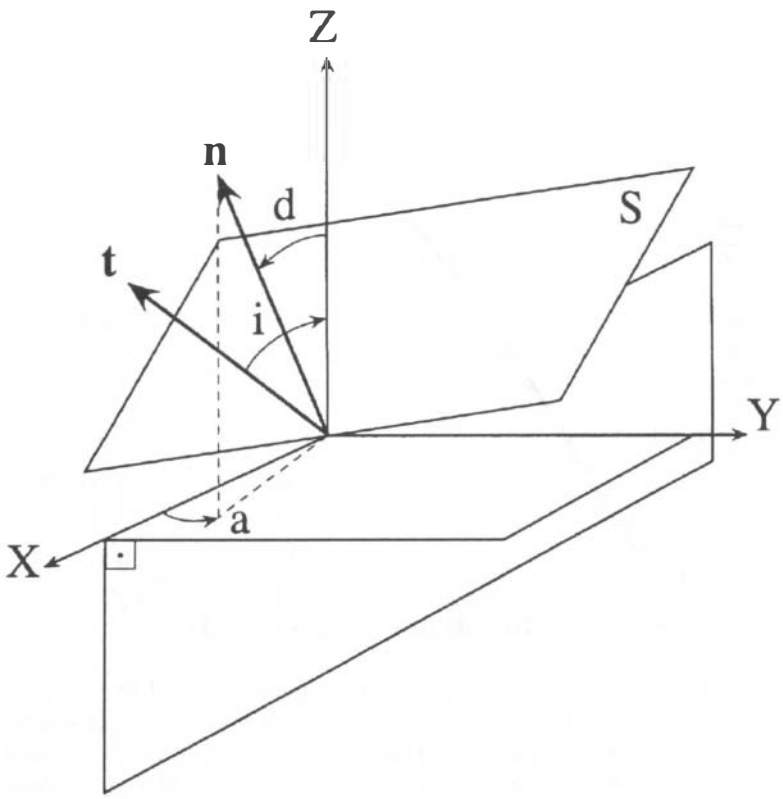

FIG. 1. Sketch illustrating the relation of coordinate system, plane S that is tangential to the slope of the mountain at the point of ray incidence and some other parameters. For details see text.

and mod A_H as function of i, d and a represent the influence of the mountain on the recorded displacement components caused by conversion coefficient.

3. RESULTS OF COMPUTATION

In this Chapter we give, as an example, mod A_H^* and mod A_V^* values as a function of i, for several combinations of d and a parameters and compare them with the mod A_H and mod A_V. For the computation we have used as the medium parameters immediately below the free–surface boundary, the density and P wave and S wave velocity that are given at the PREM model (Dziewonski and Anderson, 1981) under the boundary at the depth of 3 km.

Fig.2 gives the mod A_H and further mod A_H^* for $d = 0.5$ rad and for a equal to 0, 1, 1.5, 1.64, 2 and 3.14 rad. The mod A_H^* values depend strongly on the parameter a and for most of given values of this parameter differ significantly from

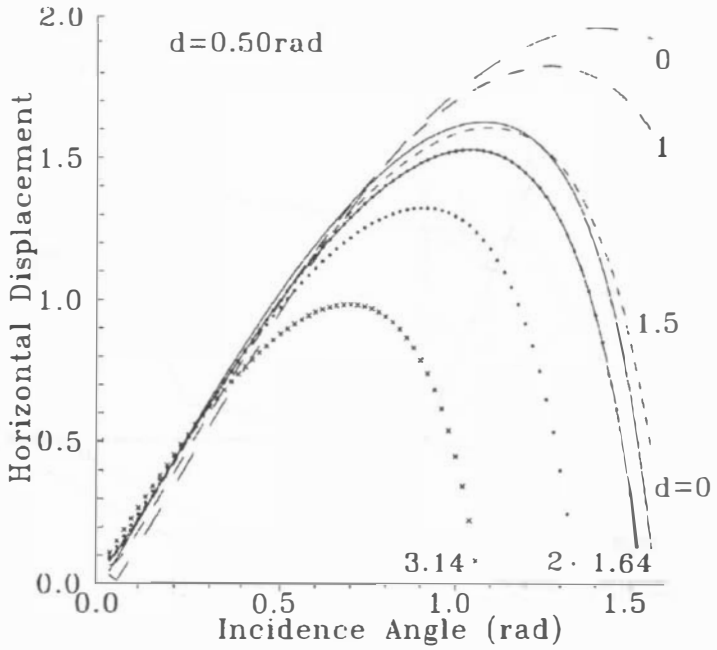

FIG. 2. The horizontal displacement component recorded by the station situated at the mountain with slope of $d = 0.5$ rad for different trends a (from 0 to 3.14rad) as the function of the incidence angle i of the ray on the horizontal surface. The same component recorded by the station situated at the horizontal surface ($d = 0$) is also given. For the medium parameters see text.

mod $\boldsymbol{A}_H$. Fig.3 gives the mod $\boldsymbol{A}_V$ and further mod $\boldsymbol{A}_V^*$ values for the same d and a as used in Fig.2. The mod $\boldsymbol{A}_V^*$ values depend on the parameter a as well, but not so strongly as the horizontal displacements in Fig.2. Only for two of given values of parameter a differ the mod $\boldsymbol{A}_V^*$ significantly from mod $\boldsymbol{A}_V$.

We consider the d value near to 0.5 rad as the maximum of realistic free–surface slope. To show the influence of lesser values of the slope on the recorded horizontal and vertical displacement, we compare in Fig.4 mod $\boldsymbol{A}_H$ with mod $\boldsymbol{A}_H^*$ and in Fig.5 mod $\boldsymbol{A}_V$ with mod $\boldsymbol{A}_V^*$ values for slope $d = 0.25$ rad. The values for parameter a are the same as used in Figs. 2 and 3. We see that the influence of mountain on the recorded horizontal and vertical displacement component is for lesser slope not so pronounced as for larger slope, but still can be significant, especially for the horizontal component.

4. RANGE OF INCIDENCE ANGLES

Figs.2 to 4 show that the influence of the mountain on the recorded horizontal and vertical displacement components are strong for larger values of wave incidence

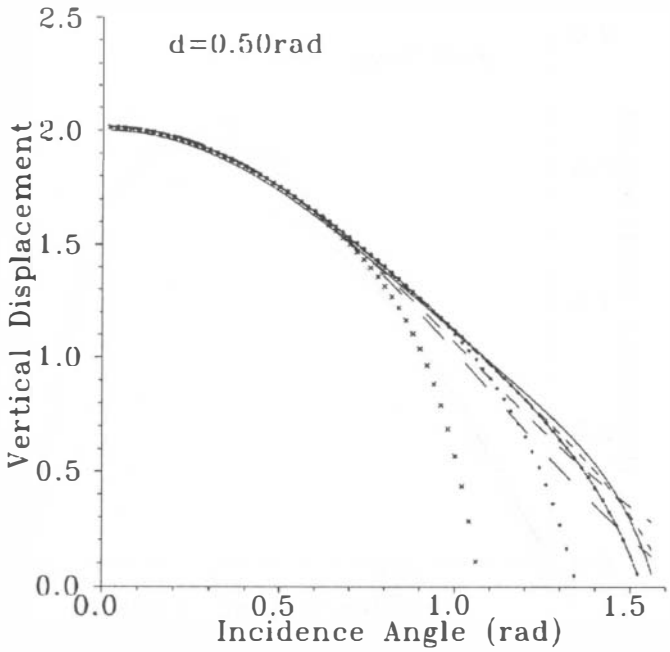

FIG. 3. The same as in Fig. 2 but for vertical component. The displacements for individual parameters a are drown in the same way as in Fig. 2.

angle and weak for small values of incidence angle.

Let us therefore discuss possible range of the incidence angle i for P waves for Earth model PREM. This model represent, in its crustal and mantle parts, a layered structure, each layer being defined by two neighbouring interfaces. This structure divides the P wave into several refracted and reflected branches. (As a reflected wave we take in consideration wave with one reflection only.) The structure of the P wave refracted and reflected branches (their number, the epicentral distance range, etc.) depend on the source depth (see e.g. Červený and Janský, 1994).

As an example, Fig.6 shows the incidence angles (for the horizontal surface) of individual P wave branches, as a function of epicentral distance for source depth of 10 km. The marks give the consecutive number of the model layer, in which rays of the corresponding P wave branch have their turning point (or minimum for the rays that are radiated from the source upwards). From Fig.6 we see that the incidence angle i can reach higher values for the branches 1 and 2 only and that the range of epicentral distance of these branches is rather narrow. For source depths below the crust the branches 1 and 2 do not exist and incidence angle is limited by value of about 0.8 rad. (Similar limitation of i as a function of epicentral distance is valid for pP and sP waves.)

We will therefore get more pronounced influence of mountain slope for small

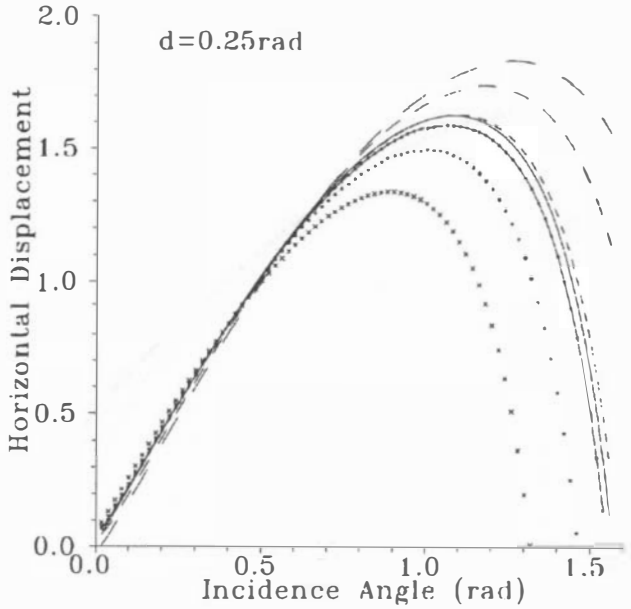

FIG. 4. The same as in Fig. 2 but for $d = 0.25$ rad.

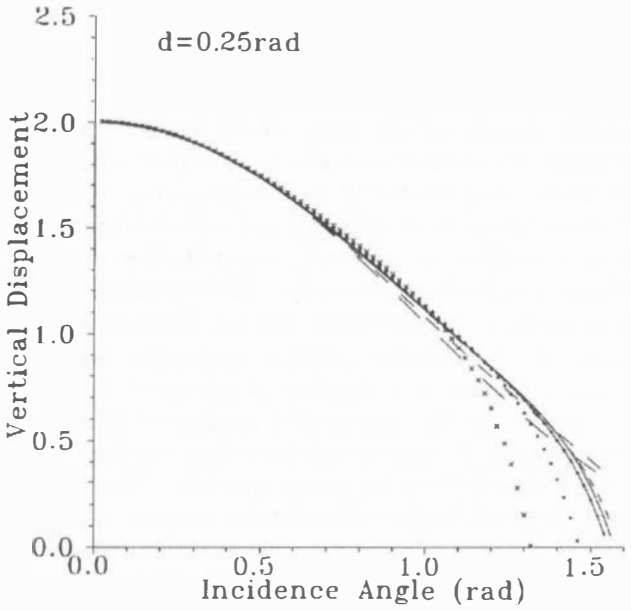

FIG. 5. The same as in Fig. 3 but for $d = 0.25$ rad.

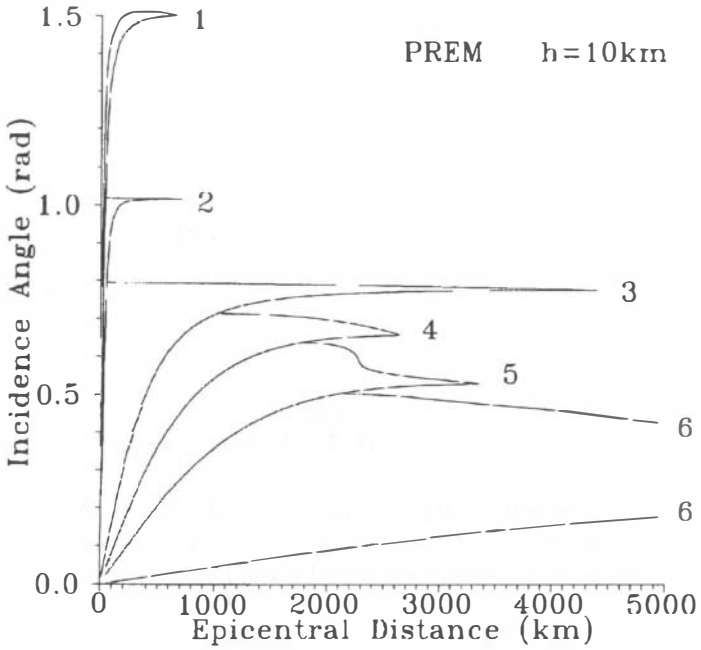

FIG. 6. Incidence angles (on the horizontal surface) of individual P wave branches as function of epicentral distance for the Earth model PREM and source depth of 10 km. Marks of individual branches gives the consecutive number of crust and mantle layer, where the rays of given branch have their deepest point. The branch 6, is not shown in full of its epicentral range.

(near) epicentral distances and shallow sources and only weaker influence for larger (teleseismic) epicentral distances or deep sources.

An example is given in Fig.7 for epicentral distance of about 400 km and in Fig.8 for epicentral distance of about 2000 km. We suppose to have there a mountain of a simple form, the cross–section of which is also given on both figures. We suppose further that the recording point is moved along the mountain (cross–section) surface with trend $a = 3.14$ up to the mountain top, and $a = 0$ afterwards. In this way we have in both cases constant i and piecewise constant a. The slope d changes with the epicentral distance. The base of mountain cross–section is 17 km long, the maximal altitude reaches 2 km. The maximal slope is 0.4 rad and is reached at the mountain (cross–section) slope inflection points. The mountain (cross–section) curvature radii are larger than 9 km.

In both figures we compare the horizontal (H) and vertical (V) displacement recorded along the mountain surface with the corresponding displacements recorded for horizontal surface, that are practically constant along the profile of 17 km.

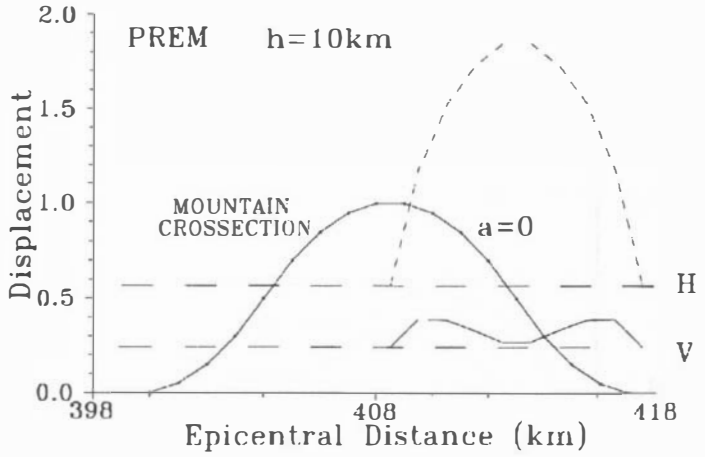

FIG. 7. The horizontal (H) – dashed line and vertical (V) – solid line displacements of the P wave, refracted branch 1, as recorded along the mountain surface of given form, at epicentral distance of 400 km from source at the depth of 10 km, model PREM. The incidence angle is near to 1.512 rad. The mountain maximal altitude is 2 km, maximal slope reaches 0.4 rad. The horizontal and vertical displacement for the case of horizontal surface are also given – long–dashed lines.

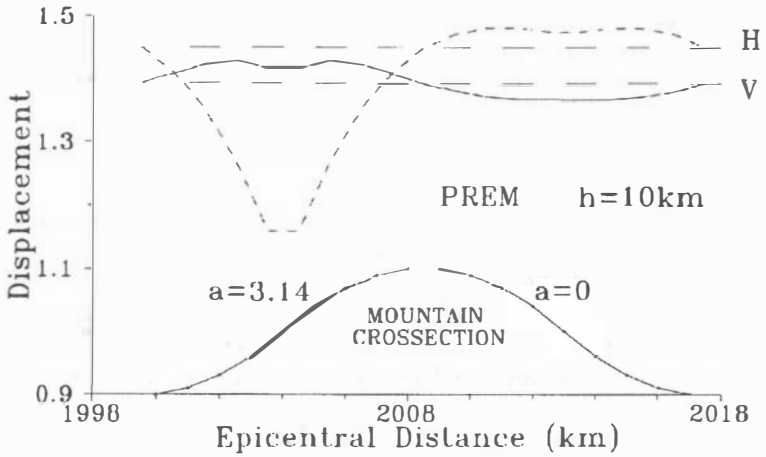

FIG. 8. The same as in Fig.7 but for refracted branch 3, at epicentral distance of 2000 km. The form of mountain surface is the same as in Fig. 7. The incidence angle is near to 0.790 rad.

In Fig.7 we give the displacements for the P wave refracted branch 1. This branch has in our example the largest horizontal and vertical displacement in the P wave group (as compared with displacement of other branches) on the record for horizontal surface and arrive about 15.9 s after the first onset. The incidence angle in this case is very large, near to 1.512 rad. From this follows that there is no incidence of this branch on the mountain surface for $a = 3.14$ rad. The horizontal displacement recorded on the mountain for $a = 0$ rad can be up to three times larger as compared with record for horizontal surface. The vertical displacement on the mountain can be up to 1.6 times larger.

In Fig.8 we give the displacements for the P wave refracted branch 3. This branch has in our example the largest horizontal and vertical displacement in the P wave group (provided the Q–factors in PREM are frequency independent) on the record for horizontal surface. It arrives about 1.6 s after the first onset. The incidence angle in this case is near to 0.790 rad. The horizontal displacement recorded on the mountain for $a = 3.14$ can be up to 1.3 times weaker as compared with record for horizontal surface. For $a = 0$ the difference between the records of horizontal displacements for mountain surface and for horizontal surface is very small. So is the difference for vertical displacement, this time for both values of a.

5. Conclusion

The mountain dimensions used in demonstration in Figs.7 and 8 can be realistic in regions of larger mountains. If we will suppose the P wave prevailing period on short period seismograph of about 0.2 – 0.3 s for epicentral distance of 400 km, we obtain for our velocity of 5.8 km/s the wave length of 1.16 – 1.73 km. This wave length is much less than the mountain base and the radii of mountain curvature. We have to expect larger prevailing period for epicentral distance of 2000 km that can be, say 0.8 – 1.0 s. This corresponds to the wave length of about 4.6 – 5.8 km. Such wave length is still more than two–times smaller than the mountain base, but is already near to the minimal radii of curvature for our model of mountain. So the application of the ray method is on its limit.

The analysis given in this contribution shows that if the seismic station is situated on the slope of a large mountain, it might be important, in special cases, to take into consideration the influence of the form of this free surface on the record of P waves, especially for the horizontal component, small epicentral distances and shallow sources.

Acknowledgements:
Thanks are due to V. Červený for encouraging this study, to J. Zahradník and two anonymous reviewers for critical comments and to M. Kvasnička for technical realization of Figures. The work was partially supported by Grant GAUK 222/95 of the Charles University, Prague.

REFERENCES

Červený, V. and Janský, J.: 1994, P and PKP amplitude–distance curves, *Acta Geophys. Polonica*, **42**, 247–272.

Dziewonski, A.N. and Anderson, D.L.: 1981, Preliminary reference Earth model, *Phys. Earth Planet. Int.*, **25**, 279–356.

Engdahl, E.R.: 1989, Coordinating global seismic network observations, *ISOP Workshop Report, EOS Trans. AGU*, **70**, 1501.

Müller, G.: Earth–flattening approximation for body waves derived from geometrical ray theory – improvements, corrections and range of applicability, *J. Geophys.*, **42**, 429–436.

Zedník, J., Janský J. and Červený, V.: 1993, Synthetic seismograms in radially inhomogeneous media for ISOP applications, *Computers & Geosciences*, **3**, 183–187.